Soft Matter

RSC Publishing

PAPER

The kinetic friction coefficient of neutral and charged polymer brushes†

Cite this: *Soft Matter*, 2013, **9**, 2966

Florent Goujon,[a] Aziz Ghoufi,[b] Patrice Malfreyt*[a] and Dominic J. Tildesley[a]

The compression-dependence of the friction coefficients of neutral and charged polymer brushes at the same surface coverage is studied using dissipative particle dynamics (DPD) at two different shear rates. The chemical potential of the solvent particles is kept constant along the compression curve in order to mimic the experimental conditions. We conclude that the kinetic friction coefficient between charged brushes is higher than that of neutral brushes at low compressions and smaller at high compressions. These differences are small. We also show that it is possible to simulate ultra-low friction coefficients comparable with experiments using the smallest shear rate accessible in a mesoscale simulation. The unexpected behavior of the shear deformation-induced structural heterogeneities in charged polymer brushes calls for further experiments to elucidate this local reorganization of the ions in adsorbed charged polymers.

Received 16th November 2012
Accepted 14th January 2013

DOI: 10.1039/c3sm27641d

www.rsc.org/softmatter

1 Introduction

Brushes are polymer chains irreversibly grafted on one end to a solid surface. At high grafting densities the polymer chains are stretched normal to the surface, giving rise to an extended structure as shown in Fig. 1. Biosensors, diagnostics, medical implants and drug delivery are examples of applications that are beginning to use polymer brushes.[1] Measurements of the frictional forces between two opposing polymer brushes under shear show them to have remarkable lubricating properties.[2–11] The first measurements,[2] carried out on mica surfaces covered by polystyrene chains in toluene, report values of friction coefficients, μ, smaller than 0.001. Later experiments[7,12] measured the normal and the shear forces of polyelectrolyte brushes in water using a surface force balance (SFB): the friction coefficient is extremely low in the range of 0.0006–0.001 for normal pressures of a few atmospheres. More recently, Chen *et al.*[9–11] were able to design polyzwitterionic brushes with chains covalently bound to the surface: these robustly surface-attached polyzwitterionic chains with no net charges and thus no free counter-ions show values of friction coefficient smaller than 0.001 up to pressures of several atmospheres. The origin of this low friction was attributed to the high level of hydration of the zwitterionic groups[10,11] on the monomers and the fluidity of the hydrating water molecules.[13,14] All these experiments show that neutral and charged polymer brushes are capable of providing excellent lubrication with $\mu < 0.001$. Recent experimental work by Liberelle and Giasson[8] on weak charged polymer brushes disagrees with most of the studies in the literature suggesting values of μ in the range of 0.05–0.25 depending on the compression. These high friction coefficients may be the result of grafting the polymer chains to the surface *via* a preexisting polymer layer: the charged polymer chain attached to one end can adsorb and form bridges with the opposing surfaces at high compressions leading to high frictional forces upon shear.[15,16]

A mechanistic understanding of the origin of the efficient lubrication of polymer brushes remains challenging[17] and still

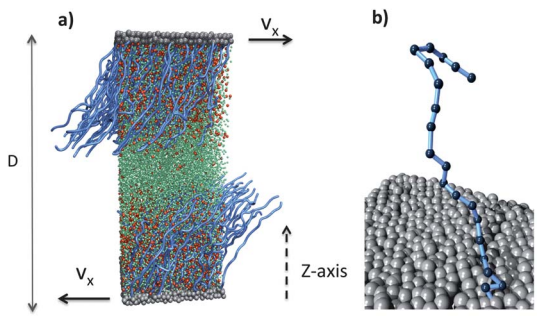

Fig. 1 (a) A typical configuration of two interacting polyelectrolyte brushes under shear at a weak compression ratio, where D is the separation distance between the two opposing brushes and v_x is the sliding velocity in the x-direction. The z-direction is the direction normal to the surfaces. The solid particles are represented in grey, the polymer beads (negatively charged) in blue, the solvent in green and the counter-ions (positively charged) in red. (b) A zoom on a given polymer chain grated to the surface without the solvent and counter-ions.

[a]*Clermont Université, Université Blaise Pascal, Institut de Chimie de Clermont-Ferrand, ICCF, CNRS, UMR 6296, BP 10448, F-63000 Clermont-Ferrand, France. E-mail: Patrice.Malfreyt@univ-bpclermont.fr; Fax: +33 473 40 53 28; Tel: +33 473407204*

[b]*Institut Physique de Rennes, IPR, CNRS, UMR 6251, 263 Avenue Général Leclerc, F-35042 Rennes, France*

† Electronic supplementary information (ESI) available: Decomposition of the profiles of the shear forces into block averages in Fig. S1. See DOI: 10.1039/c3sm27641d

rather incomplete because we do not have precise structural measurements of the polymer, solvent and counter-ions under shear. Actually, when two polymer brushes (Fig. 1) interact, a large number of factors such as the solvent quality, the salt concentration, the nature of the polymer (charged or neutral), the compression, the shear-velocity and the detachment of chains from surfaces[18] can change the frictional forces. The surface force apparatus can be used to determine the friction coefficient between grafted polyelectrolytes experimentally,[7,8,15] but there is some uncertainty in maintaining the grafting density under shear at high compressions and small separation distances.[8] During the last decade, numerous theoretical and computational studies have been performed to elucidate the mechanism responsible for low friction between polymer brushes. There are many excellent theoretical[19–25] and computer simulation studies[22,26–34] on the behavior of polyelectrolyte brushes at equilibrium. The challenge is to extend these insights to sliding layers.[32–36] The main obstacle for the molecular simulation methods is to reach the required length and time scales to study the physics of these adsorbed chains, and this suggests the use of a mesoscale simulation technique such as dissipative particle dynamics (DPD), which allows us to extend the time scales without abandoning the particle description of the problem. The first advantage of DPD[37,38] is that it can use time steps up to an order of magnitude larger than those typically used in MD simulations.[32–34] Secondly, and unlike the Brownian dynamics (BD), hydrodynamic interactions are properly accounted for. Thirdly, it is straightforward to model the solvent particles explicitly.[31,39–41] Recent progress in DPD simulations allowed us to modify the standard DPD algorithm by the addition of forces preventing bond crossing between polymers[42–44] and electrostatic interactions to model polyelectrolytes.[35,36,45–49]

DPD has been successfully applied to investigate a variety of soft matter problems such as the microphase separation of a block copolymer,[50,51] polymer surfactant in solution,[52] and the structure and rheology of biological membranes.[37] In the past, we successfully applied the dissipative particle dynamics (DPD) method to study the equilibrium properties[39,40,42] and rheological properties[41,44,53] of neutral polymer brushes. The dependence of the brush height with respect to the surface coverage[48] is found to follow the theoretical prediction.[54,55] DPD simulations in the grand canonical ensemble[40–42,44] were carried out to calculate the force profiles as a function of the separation distance between the two brushes. Comparison with experiments has shown that the DPD simulations were able to reproduce the main structural and rheological properties of the neutral brushes under compression. The force–distance profiles of neutral polymer brushes calculated from DPD simulations are in very good agreement with the self-consistent field (SCF) theoretical models[54,56] and experimental results[57] for two polystyrene brush layers grafted onto mica surfaces in toluene. We have also performed mesoscale simulations[47] of a polyelectrolyte brush in athermal solvent conditions in order to study the impact of the grafting density, the charge fraction and the salt concentration on the structural properties of a single brush. The DPD simulations predict a parabolic shape for the monomer density profiles, in contrast to that predicted by previous computer simulations where the solvent was not treated explicitly. The parabolic profile of polyelectrolyte brushes calculated from DPD simulations is in agreement with that determined from neutron reflectivity measurements[58] and density functional theory calculations.[59] The dependence of the brush height with respect to the grating density is found to be identical to that predicted by the scaling law of the nonlinear osmotic brush regime.[22,26,60] We have shown that the DPD simulations accurately reproduce the theoretical dependence of the brush height with respect to the charge fraction in the nonlinear osmotic brush regime. The main conclusions we can draw from our mesoscale simulations of single and interacting polyelectrolyte brushes are as follows: (i) the dependence of the brush height on the grafting density and of the charge fraction is typical of the nonlinear osmotic brush regime,[22,26,29] (ii) all the counter-ions are confined inside of the brush in agreement with the small values of the Gouy–Chapman length,[47–49] (iii) the interpenetration coefficient between two interacting polyelectrolyte brushes follows the scaling law of the nonlinear osmotic brush regime,[49,61] (iv) the normal pressure between two interacting brushes follows the dependence expected from the scaling law of the pressure in the osmotic regime.[20] DPD simulations were also carried out to investigate the dependence of the interpenetration coefficient on the grafting density, polymer size and separation distance.[35] Recently, a scaling theory was developed from the results of DPD simulations and experiments to model the behavior of two interacting polymer brushes.[31]

The present paper represents a significant extension of our previous study[36] of this system. Here, we propose to determine the friction coefficient between neutral and charged polymer at the same point along the compression curve and for two different shear rates. We aim to mimic the experimental conditions used in the surface force balance (SFB) measurements[62] by modeling the two interacting polymer brushes in the grand canonical ensemble where the chemical potential of the solvent is kept constant for all the compressions. We aim to model the lowest possible shear rates before the off-diagonal component of the stress tensor disappears into the noise by using exceptionally long simulation runs.

This means that the non-equilibrium DPD simulations reported here are performed at fixed solvent chemical potential along the compression curve. The key question that we wish to address using our simulation techniques is: how does the friction change with the compression when comparing neutral and charged polymer brushes in a good solvent? In particular, how and to what extent does the introduction of charge change the friction along the compression curve? To this end, we will establish the effect of shear on the brush structure, and we will calculate the components of the stresses between the solid surfaces, the viscosity and the overlap or interpenetration between the two brushes along the compression curve.

In the next section, we briefly describe the DPD model used and the computational procedures. The results are discussed in Section 3 and we give the main conclusions of this work in Section 4.

2 Computational procedures

2.1 DPD model

In the DPD model used here, solvent and polymer particles are coarse grained into soft beads. The total force acting on the i^{th} particle becomes

$$f_i = \sum_{j\neq i}^{N}\left(f_{ij}^{C} + f_{ij}^{R} + f_{ij}^{D} + f_{ij}^{E}\right) + \sum_{k\neq i}^{N_c}\left(f_{ik}^{S}\right) \quad (1)$$

where N is the total number of beads in the system and N_c is the number of connected polymer beads. The pairwise electrostatic f_{ij}^{E} force is then added to the sum of the conservative f_{ij}^{C}, dissipative f_{ij}^{D} and random f_{ij}^{R} pairwise forces. The spring f_{ik}^{S} force ensures the integrity of the polymer chain. The reader is directed to ref. 36 and 47–49 for a comprehensive description of these forces.

2.2 Simulation details

2.2.1 Description of the system. The chains are formed of 20 negatively charged polymer beads and are chemically end-grafted to the solid surface. Comparison with experiments[8] suggests that each polymer bead represents up to 8 monomer units. The shear $\dot{\gamma}_a$ is applied by moving the top and bottom surface particles in opposite directions along x. The system of grafted bilayers consists of two hexagonal planar surfaces, each composed of two layers of 598 DPD particles. The two surfaces are coated with 100 polymer chains that are randomly grafted by a harmonic force acting between the particles of the chains and the particles of the first layer of the surface. The surface coverage defined by the ratio of the number of grafted chains to the surface area is 0.5 in reduced units. This means that the fraction of wall particles of the last layer connected to the first beads of the polymer chains is 1/6. The dimensions of the brushes simulated here match those used in experiments: the ratio of the inter-chain distance to the Flory radius is equal to 0.3 and 0.4 for simulations and experiments, respectively.[8] This surface coverage places the chain in the nonlinear osmotic brush regime[48] where they are essentially normal to the surface at equilibrium. When polyelectrolyte brushes are modelled, 4000 counter-ions, which are positively charged are added to preserve the neutrality. The energy parameters are set to 20.0 for the polymer–solvent interactions and to 25.0 for all the other interactions. This means that the polymer brushes are modelled under good solvent conditions. The DPD simulations consist of an equilibration period of 1.5×10^6 steps followed by an acquisition period of 500 000 to 1.0×10^6 steps. The reader is directed to ref. 36 for a complete description of the model and computational procedures.

2.2.2 Grand canonical statistical ensemble. The DPD simulations were formed in the grand canonical ensemble where the chemical potential of the solvent is kept constant for all the compressions. The reference chemical potential was calculated by particle insertion at the separation distance D_0 which corresponds to the minimum separation distance of a grafted bilayer in which the shape of the monomer density profile and the brush height are strictly identical to those calculated in a single brush. The chemical potential calculated at D_0 was equal to 18.0 in reduced DPD units for the charged and neutral polymer chains. The condition of constant chemical potential can be readily included in DPD simulations[40] by performing creation/deletion moves of solvent particles occasionally (*i.e.*, we do not want to destroy the dynamics[41] with too many creations and deletions). The acceptance probabilities for a trial creation or deletion of a solvent particle become

$$P_{\text{creation}}^{\text{acc}} = \min\left[1, \frac{\langle Z\rangle V}{N+1}\exp\left(-\frac{\Delta U}{kT}\right)\right] \quad (2)$$

$$P_{\text{deletion}}^{\text{acc}} = \min\left[1, \frac{N}{\langle Z\rangle V}\exp\left(-\frac{\Delta U}{kT}\right)\right] \quad (3)$$

where V is the total volume of the box, T is the temperature and N is the total number of particles before the move. ΔU is the energy between the added or removed particle and the N or $N-1$ remaining particles, calculated using the conservative potential. $\langle Z\rangle$ is the local activity of the solvent defined as $\exp(\mu^{\text{conf}}/k_BT)$ where μ^{conf} is given as

$$\mu^{\text{conf}} = \left\langle \mu^{\text{conf}}(z)\right\rangle_z = \left\langle k_BT \ln\left[\frac{\langle\rho(z)\rangle}{\left\langle \exp\left(-\frac{\Delta U^{\text{test}}}{k_BT}\right)\right\rangle}\right]\right\rangle_z \quad (4)$$

where $\rho(z)$ is the number density of the solvent particle and $\mu^{\text{conf}}(z)$ is the configurational chemical potential at height z. The chemical potential calculated through eqn (4) is constant at every z.[41] When a creation attempt is accepted, the velocity of the corresponding particle is chosen from a Gaussian distribution with zero mean and $\sqrt{k_BT}$ variance. When the shear is applied along the x-direction, the x-component of the solvent particle's velocity is changed by the addition of the x-component of the streaming velocity. When a deletion attempt is successful, the solvent particle is removed.

2.3 Calculation of the stress, friction and viscosity

The components of the pressure tensor used for the determination of the friction coefficient are calculated along the z-axis using the Irving–Kirkwood[63,64] definition. The profiles of the pressure are calculated by splitting the cell into slabs of width Δz. The $p_{\alpha\beta}$ component is defined as

$$p_{\alpha\beta}(z) = \frac{1}{V}\left\langle \sum_{i,\alpha,\beta} H(z_i) m_i \left[(v_i)_\alpha - (u)_\alpha\right]\left[(v_i)_\beta - (u)_\beta\right]\right\rangle + \frac{1}{A}\left\langle \sum_{i=1}^{N-1}\sum_{j>i}^{N} (r_{ij})_\alpha (f_{ij})_\beta \frac{1}{|z_{ij}|}\theta\left(\frac{z-z_i}{z_{ij}}\right)\theta\left(\frac{z_j-z}{z_{ij}}\right)\right\rangle \quad (5)$$

where $\langle\ldots\rangle$ denotes the configurational average, α and β represent the x, y and z directions, and m_i and $(v_i)_\alpha$ are the mass and velocity of particle i, respectively. $V = L_xL_y\Delta z$ is the volume of the basic slab, $H(z_i)$ is a top-hat function and $(u)_\alpha$ is the α component of the streaming velocity. Whereas $(u)_x$ is a measure of the induced flow field, $(u)_y$ and $(u)_z$ are essentially zero for all z. f_{ij} represents the sum of the pairwise additive forces and θ is a unit step function. The friction coefficient defined in eqn (6) is

averaged over the slabs along the z-direction as the ratio of the off-diagonal pressure tensor component in the shear direction to the normal component $p_N(z) = p_{zz}(z)$

$$\langle \varepsilon \rangle = \langle \varepsilon(z) \rangle_z = \left\langle -\frac{p_{xz}(z)}{p_{zz}(z)} \right\rangle_z . \quad (6)$$

The shear viscosity is calculated in the middle of the simulation cell from the profile of $\eta(z)$ as

$$\eta(z) = -\frac{\langle p_{xz}(z) \rangle}{\left\langle \frac{\mathrm{d}u_x(z)}{\mathrm{d}z} \right\rangle} . \quad (7)$$

3 Results and discussions

To begin, we focus on the smallest value of shear rate we can use with the DPD simulations in order to calculate a reliable friction coefficient. The shear rates used in the simulations are in the range of 10^{-4} to 10^{-1} in reduced units. The value of 10^{-4} corresponds to a real shear rate of 10^6 s^{-1} if we take the time step to be 10 ps (ref. 37 and 38) and the unit of size[37] r_c to be 6 Å. (These values were calculated from the diffusion coefficient of water in ref. 37.) From these values, the reduced unit of pressure at 298 K corresponds to about 10 MPa. These shear rates are two orders of magnitude smaller than those used with molecular dynamics simulations[32–34] and two orders of magnitude larger than those used in experiments.[2,15] The reduced shear rate of 10^{-4} is the smallest value we can simulate with DPD models. For shear rates lower than 10^{-4}, the standard error in the mean of $-\langle p_{xz} \rangle$ overlaps significantly with the standard error in the mean of $-\langle p_{xz} \rangle = 0$ for systems without shear. This makes an estimate of the friction coefficient at this value of v_x. Given sufficiently long runs, it would be possible to reduce these errors and therefore v_x slightly. However, the simulation of one charged system requires at the lowest shear rate studied 125 cpu hours for 20 000 particles over 3×10^6 time steps. This makes further significant reduction in v_x very difficult given our current resources. The reader is redirected to Fig. S1 in the ESI† for an analysis of the profiles of p_{xz} at the smallest shear rate and at equilibrium. Fig. 2a shows a linear dependence of the friction coefficient on the shear rate, whereas Fig. 2b, for the normal pressure, shows no shear rate dependence. The faster the surfaces are slid past one another, the higher the shear forces. In the light of these results, we decided to compare the friction coefficient between neutral and charge brushes along the compression curve for $\dot{\gamma}_a = 0.0025$ and $\dot{\gamma}_a = 0.1$.

Fig. 3 shows the density profiles of neutral and charged polymer brushes at equilibrium and under shear. The shear acts to retract the brushes, decreasing the interpenetration between the two opposing brushes and shifting the solvent into the overlap region. For neutral brushes, the monomer density profiles (corresponding to the polymer chains) become increasingly parabolic under shear (see Fig. 3a and c). For equilibrium polyelectrolyte brushes, the profile in Fig. 3b of the counter-ions matches, almost exactly, that of the polymer, indicating that the counter-ions are trapped within the brush layers. Local charge neutrality (Fig. 3b) is observed in this region when no shear is applied. The density profiles of the solvent particles show that the polymer beads attract the solvent particles into the region between the polymers and the polymer beads extend away from the surface as expected in a good solvent.

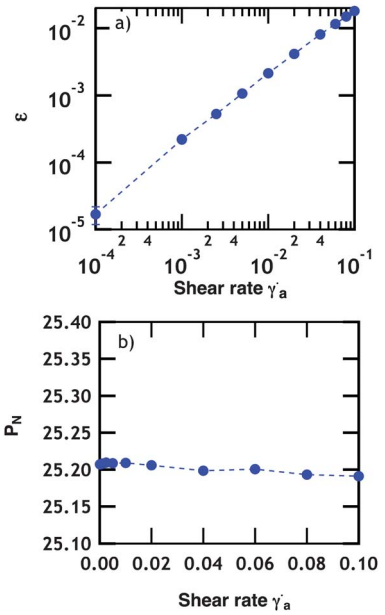

Fig. 2 Dependence of (a) the friction coefficient and (b) normal force ($p_{zz} = p_N$) as a function of the shear rate $\dot{\gamma}_a$ for neutral polymer brushes at $D/D_0 = 1.0$.

Interestingly, the shear significantly affects the density profiles of charged monomers by creating some heterogeneity in the shape of the polymer brushes. Some chains are forced to fold in order to maintain a local neutrality with a smaller number of counter-ions around the chains and an excess of counter-ions with respect to polymer beads is then observed in the central region (Fig. 3d). The increase in density of the counter-ions in the center of the box is at the expense of the ions just inside the brush structure creating an oscillatory profile. Ions close to the interface can move more easily and preserve

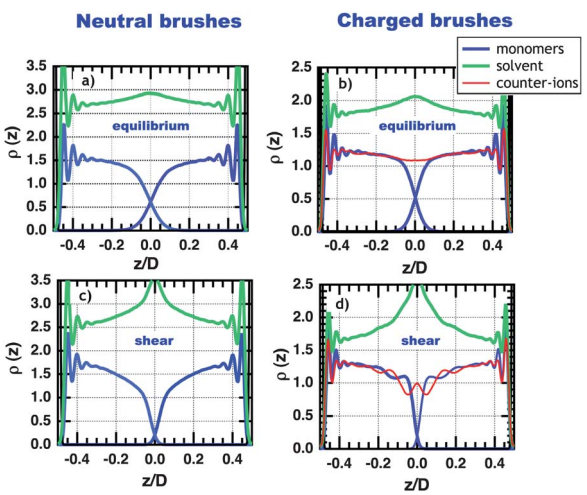

Fig. 3 Monomer, solvent and counter-ion density profiles along the normal to the surfaces as a function of the reduced z/D quantity for neutral and charged polymer brushes at $D/D_0 = 0.5$ at equilibrium and under shear for $\dot{\gamma}_a = 0.1$.

local electroneutrality because of the flexibility of the brushes at the interface. The shear changes the structure of the charged polymer brushes from those of neutral brushes at the same shear and compression.

We plot in parts (a) and (b) of Fig. 4 the friction coefficient defined in eqn (6) as a function of the compression ratio for two different shear rates. We also plot the differences between the pressure at a given separation distance D and the pressure at D_0 for the normal and tangential components along the compression profile. Fig. 4a and b establish that the friction coefficient between neutral and charged brushes is of the same order of magnitude in agreement with recent experiments[2,9–11] on polyzwitterionic brushes. We also show that it is possible to reach values of friction comparable to experiments with small shear rates. The difference in friction between charged and uncharged polymer brushes does not depend on the sliding velocity.

At low compressions ($D/D_0 > 0.5$), the increase in ε with D (Fig. 4a and b) of polyelectrolyte brushes is slightly faster than that observed for neutral brushes. This phenomenon is accentuated at higher shear rates as observed in Fig. 4b. This is due to the larger value of the shear force (shown in Fig. 4d) in the polyelectrolyte brushes. The normal force is independent of D at these compression ratios. This suggests that the counter-ions inside the brushes reinforce the interaction between the monomers of the different chains by acting as a glue and that this increases the force required to slide the surfaces past each other under the same normal load. Actually, the polyelectrolyte brushes are less susceptible to tilt in shear flows than neutral brushes in agreement with the behavior predicted by theory.[65] The average tilt of the layer is about 36° for neutral brushes and 42° for charged brushes for $D/D_0 > 0.5$.

At separation distances less than $D/D_0 > 0.5$, the friction is lower for the polyelectrolyte brushes at high compressions. The friction tends towards a plateau with decreasing D/D_0 at lower values of ε. At a given compression ratio in the strong compression regime ($D/D_0 < 0.5$), Fig. 4c and d establish that the change in the friction coefficient with the compression ratio between neutral and polyelectrolyte brushes is mainly caused by the change in the normal force and not by the change in the shear force. The difference in the normal force between charged and neutral brushes is caused by the repulsion between the charged polymer chains screened by the layers of counter-ions between the brushes. The origins of this change in the friction can be seen in the correlations between the normal load, the viscosity and the interpenetration of the two brushes. We show the viscosity in the middle of the pore as a function of the normal pressure in Fig. 5a for charged and uncharged polymer brushes. The viscosity is calculated using eqn (7). In this pressure range, we observe that the polyelectrolyte brushes show values of viscosity in the overlap region that are slightly smaller than those of the neutral brushes. Additionally, the difference in viscosity between neutral and charged brushes increases with the normal pressure. The solvent-rich region between the two interacting brushes is then more fluid and can serve as an efficient lubricating layer. The presence of an excess of counter-ions in this region results in an increase of the charge layer just above the brush and in a decrease in the viscosity. Concerning the role played by the neutral solvent particles, we examine polymer brushes with and without solvent particles. For the same separation ($D/D_0 = 0.4$), the solvent particles reduce the friction coefficient by factors of 2.0 and 1.4 with respect to solvent-free brushes (dry brushes) in both neutral and charged

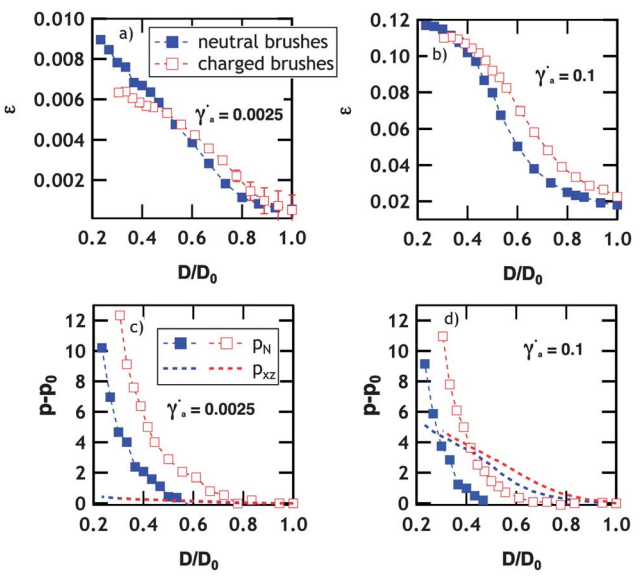

Fig. 4 Friction coefficient, shear and normal forces as a function of the compression ratio D/D_0 calculated for neutral and charged polymer brushes for two shear rates. $p - p_0$ is calculated for the normal and tangential pressure where $p_{xz,0}$ and $p_{zz,0}$ are the tangential and normal components of the pressure tensor in the polymer brushes at $D = D_0$, respectively. The standard errors in p_{xz}, in the order of 10^{-3} in reduced units, are smaller than the symbols.

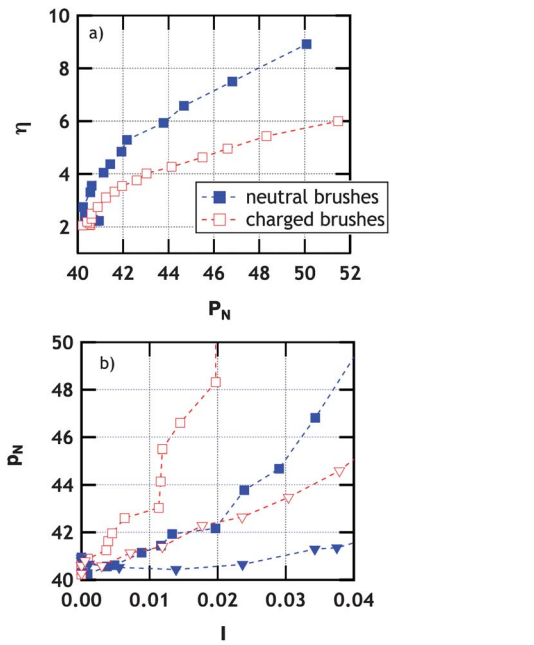

Fig. 5 (a) Viscosity of the solvent in the overlap region as a function of the normal pressure. (b) Normal pressure as a function of the interpenetration coefficient between the two interacting brushes. The square symbols represent the higher shear rate and the triangles the smaller.

brushes, respectively. This decrease in the friction illustrates the lubricant properties of the solvent particles that tend to solvate the polymer beads and the counter-ions leading to the formation of hydration sheaths.[7,10,11] This effect may be more dramatic if the polarizability of the solvent is considered.

Fig. 5b reports the normal pressure as a function of the interpenetration coefficient I between the two interacting brushes. This coefficient quantifies the overlap between the two sheared brushes and is defined as

$$I = \frac{\int_{0}^{L_z/2} \rho_1(z)\mathrm{d}z}{\int_{-L_z/2}^{L_z/2} \rho_1(z)\mathrm{d}z} \quad (8)$$

where $\rho_1(z)$ is the density profile of one brush. The interpenetration coefficient is then averaged over the two brushes. For a given overlap, Fig. 5b establishes that the polyelectrolyte brushes can support a larger load than that in neutral brushes independently of the shear rate. For the same applied load, we observe in Fig. 5b that the interpenetration is smaller in charged brushes than in neutral ones. These two observations find their origin in the presence of free counter-ions, which contributes to the osmotic pressure within the brush.

4 Conclusions

We have calculated the kinetic friction coefficient of neutral and charged polymer brushes with the same grafting density at different compression ratios in an effort to model SFB experiments in these systems. We have shown that the smallest shear rates we can apply to the brushes by using DPD models are of the order of 10^6 s^{-1}. Below this value, the calculation of the shear force does not allow an accurate calculation of the friction.

The main results we can draw from this work can be summarized as follows: (i) the kinetic friction coefficient of neutral and charged polymers is of the same order of magnitude at the same point of the compression curve. This is in line with most of the experimental studies on neutral,[2] charged[7,12] and zwitterionic[10,11] polymer brushes. Additionally, it is possible to calculate ultra-low kinetic friction coefficients of the same order of magnitude as observed in the experiments provided that we used the lowest shear rate possible in the DPD simulation even if the shear rate used in DPD is two orders of magnitude larger than those used in SFB experiments but two orders of magnitude smaller than those used in most atomistic simulations. (ii) The friction between polyelectrolyte brushes stops increasing at lower values of the compression compared to neutral brushes. In contrast, the friction in polyelectrolyte brushes is larger than in neutral brushes at weak compressions and smaller at strong compressions, although the differences remain small. (iii) The polyelectrolyte brushes can support a higher load due to the presence of free counter-ions within the brush. The viscosity in the polymer free gap is smaller in charged brushes than in neutral brushes, indicating that the solvent particles in this region assist the sliding of the two interacting charged brushes. (iv) The unexpected behavior of the shear deformation-induced structural heterogeneities in charged polymer brushes calls for further experiments to elucidate this local reorganization of the ions in adsorbed charged polymers.

Acknowledgements

For this work, the authors were granted access to the HPC resources of IDRIS under the allocation 2012-i2012092119 made by GENCI (Grand Equipement National de Calcul Intensif). The authors are grateful for the financial support of the CNRS for the PEPS-PTI 2012 project entitled “Multiscale modelling of polymeric materials for the transport of electrolytes”.

References

1 M. Welch, A. Rastogi and C. Ober, *Soft Matter*, 2011, **7**, 297.
2 J. Klein, E. Kumacheva, D. Mahalu, D. Perahia and L. J. Fetters, *Nature*, 1994, **370**, 634.
3 R. Tadmor, J. Janik and J. Klein, *Phys. Rev. Lett.*, 2003, **91**, 115503.
4 S. M. Kilbey, F. S. Bates, M. Tirrell, H. Yoshizawa, R. Hill and J. Israelachvili, *Macromolecules*, 1995, **28**, 7107.
5 P. A. Schorr, T. C. B. Kwan, S. M. Kilbey, E. S. G. Shaqfey and M. Tirrell, *Macromolecules*, 2003, **36**, 389.
6 U. Raviv, J. Frey, R. Sak, P. Laurat, R. Tadmor and J. Klein, *Langmuir*, 2002, **18**, 7482.
7 U. Raviv, S. Giasson, N. Kampf, J. F. Gohy, R. Jerome and J. Klein, *Nature*, 2003, **425**, 163.
8 B. Liberelle and S. Giasson, *Langmuir*, 2008, **24**, 1550.
9 M. Chen, W. H. Briscoe, S. P. Armes, H. Cohen and J. Klein, *ChemPhysChem*, 2007, **8**, 1303.
10 M. Chen, W. H. Briscoe, S. P. Armes and K. Klein, *Science*, 2009, **23**, 1698.
11 M. Chen, W. H. Briscoe, S. P. Armes, H. Cohen and J. Klein, *Eur. Polym. J.*, 2011, **47**, 511.
12 U. Raviv, S. Giasson, N. Kampf, J. F. Gohy, R. Jerome and K. Klein, *Langmuir*, 2008, **24**, 8678.
13 U. Raviv, P. Laurat and J. Klein, *Nature*, 2001, **413**, 51.
14 U. Raviv and J. Klein, *Science*, 2002, **297**, 1540.
15 I. E. Dunlop, W. H. Briscoe, S. Titmuss, R. M. J. Jacobs, V. L. Osborne, S. Edmondson, W. T. S. Huck and J. Klein, *J. Phys. Chem. B*, 2009, **113**, 3947.
16 I. E. Dunlop, R. K. Thomas, S. Titmus, V. L. Osborne, S. Edmondson, W. T. S. Huck and J. Klein, *Langmuir*, 2012, **28**, 3187.
17 L. Spirin, A. Galuschko, T. Kreer, K. Binder and J. Baschnagel, *Phys. Rev. Lett.*, 2011, **106**, 168301.
18 F. Goujon, P. Malfreyt and D. J. Tildesley, *Soft Matter*, 2010, **6**, 3472.
19 S. Misra, S. Varanasi and P. P. Varanasi, *Macromolecules*, 1989, **22**, 4173.
20 P. Pincus, *Macromolecules*, 1991, **24**, 2912.
21 O. V. Borisov, E. B. Zhulina and T. M. Birshtein, *Macromolecules*, 1994, **27**, 4795.
22 H. Ahrens, S. Förster, C. A. Helm, N. A. Kumar, A. Naji, R. R. Netz and C. Seidel, *J. Phys. Chem. B*, 2004, **108**, 16870.

23 J. B. Sokoloff, *Macromolecules*, 2002, **40**, 4053.
24 J. B. Sokoloff, *J. Chem. Phys.*, 2008, **129**, 014901.
25 M. W. Matsen, *Eur. Phys. J. E*, 2012, **35**, 13.
26 A. Naji, R. R. Netz and C. Seidel, *Eur. Phys. J. E*, 2003, **12**, 223.
27 F. S. Csajka and C. Seidel, *Macromolecules*, 2000, **33**, 2728.
28 C. Seidel, *Macromolecules*, 2003, **36**, 2536.
29 N. A. Kumar and C. Seidel, *Macromolecules*, 2005, **38**, 9341.
30 O. J. Hehmeyer and M. J. Stevens, *J. Chem. Phys.*, 2005, **122**, 134909.
31 A. Galuschko, L. Spirin, T. Kreer, A. Johner, C. Pastorino, J. Wittmer and J. Baschnagel, *Langmuir*, 2011, **26**, 6418.
32 D. Russano, J. M. Y. Carrillo and A. V. Dobrynin, *Langmuir*, 2011, **27**, 11044.
33 J. M. Y. Carrillo, D. Russano and A. V. Dobrynin, *Langmuir*, 2011, **27**, 14599.
34 Y. Ou, J. B. Sokoloff and M. J. Stevens, *Phys. Rev. E*, 2012, **85**, 011801.
35 M. Sirchabesan and S. Giasson, *Langmuir*, 2007, **23**, 9713.
36 F. Goujon, A. Ghoufi, P. Malfreyt and D. J. Tildesley, *Soft Matter*, 2012, **8**, 4635.
37 R. D. Groot and K. L. Rabone, *Biophys. J.*, 2001, **81**, 725.
38 G. Maurel, B. Schnell, F. Goujon, M. Couty and P. Malfreyt, *J. Chem. Theory Comput.*, 2012, **8**, 4570.
39 P. Malfreyt and D. J. Tildesley, *Langmuir*, 2000, **16**, 4732.
40 F. Goujon, P. Malfreyt and D. J. Tildesley, *ChemPhysChem*, 2004, **5**, 457.
41 F. Goujon, P. Malfreyt and D. J. Tildesley, *Mol. Phys.*, 2005, **103**, 2675.
42 F. Goujon, P. Malfreyt and D. J. Tildesley, *J. Chem. Phys.*, 2008, **129**, 034902.
43 F. Lahmar, C. Tzoumanekas, D. N. Theodorou and B. Rousseau, *Macromolecules*, 2009, **42**, 7485.
44 F. Goujon, P. Malfreyt and D. J. Tildesley, *Macromolecules*, 2009, **42**, 4310.
45 R. D. Groot, *J. Chem. Phys.*, 2003, **118**, 11265.
46 M. Gonzalez-Melchor, E. Mayoral, M. E. Velazquez and J. Alejandre, *J. Chem. Phys.*, 2006, **125**, 224107-1.
47 C. Ibergay, P. Malfreyt and D. J. Tildesley, *J. Chem. Theory Comput.*, 2009, **5**, 3245.
48 C. Ibergay, P. Malfreyt and D. J. Tildesley, *J. Phys. Chem. B*, 2010, **114**, 7274.
49 C. Ibergay, P. Malfreyt and D. J. Tildesley, *Soft Matter*, 2011, **7**, 4900.
50 R. D. Groot and T. J. Madden, *J. Chem. Phys.*, 1998, **108**, 8713.
51 R. D. Groot, T. J. Madden and D. J. Tildesley, *J. Chem. Phys.*, 1999, **110**, 9739.
52 R. D. Groot, *Langmuir*, 2000, **16**, 7493.
53 D. Irfachsyad, D. J. Tildesley and P. Malfreyt, *Phys. Chem. Chem. Phys.*, 2002, **4**, 3008.
54 S. Alexander, *J. Phys.*, 1977, **38**, 983.
55 S. T. Milner, *Science*, 1991, **251**, 905.
56 P. G. de Gennes, *Adv. Colloid Interface Sci.*, 1987, **21**, 2610.
57 H. J. Taunton, C. Toprakcioglu, L. J. Fetters and J. Klein, *Macromolecules*, 1990, **23**, 571.
58 G. Romet-Lemonne, J. Daillant, P. Geunoun, J. Yang and J. W. Mays, *Phys. Rev. Lett.*, 2004, **93**, 148301.
59 T. Jiang and J. Wu, *J. Phys. Chem. B*, 2008, **112**, 7713.
60 A. Naji, C. Seidel and R. R. Netz, *Adv. Polym. Sci.*, 2006, **198**, 149.
61 N. A. Kumar and C. Seidel, *Phys. Rev. E*, 2007, **76**, 020801.
62 J. Klein and E. Kumacheva, *J. Chem. Phys.*, 1998, **108**, 6996.
63 J. P. R. B. Walton, D. J. Tildesley, J. S. Rowlinson and J. R. Henderson, *Mol. Phys.*, 1983, **48**, 1357.
64 J. P. R. B. Walton, D. J. Tildesley and J. S. Rowlinson, *Mol. Phys.*, 1986, **58**, 1013.
65 J. L. Harden, O. V. Borisov and M. E. Cates, *Macromolecules*, 1997, **30**, 1179.